ELSEVIER

Journal of Nuclear Materials 265 (1999) 262–272

journal of nuclear materials

Effect of heat treatment and irradiation temperature on impact properties of Cr–W–V ferritic steels [1]

R.L. Klueh *, D.J. Alexander

Metals and Ceramics Division, Oak Ridge National Laboratory, P.O. Box 2008, MS 6376, Oak Ridge, TN 37831-6376, USA

Received 2 June 1998; accepted 26 October 1998

Abstract

Charpy impact tests were conducted on eight normalized-and-tempered ferritic and martensitic steels irradiated in two different normalized conditions. Irradiation was conducted in the Fast Flux Test Facility (FFTF) at 393°C to ≈14 dpa on eight steels with 2.25%, 5%, 9%, and 12% Cr (0.1% C) with varying amounts of W, V, and Ta. The different normalization treatments involved changing the cooling rate after austenitization. The faster cooling rate produced 100% bainite in the 2.25Cr steels, compared to duplex structures of bainite and polygonal ferrite for the slower cooling rate. For both cooling rates, martensite formed in the 5% and 9% Cr steels, and martensite with ≈25% δ-ferrite formed in the 12% Cr steel. Irradiation caused an increase in the ductile–brittle transition temperature (DBTT) and a decrease in the upper-shelf energy (USE). The difference in microstructure in the low-chromium steels due to the different heat treatments had little effect on properties. For the high-chromium martensitic steels, only the 5Cr steel was affected by heat treatment. When the results at 393°C were compared with previous results at 365°C, all but a 5Cr and a 9Cr steel showed the expected decrease in the shift in DBTT with increasing temperature.

1. Introduction

Reduced-activation or fast induced-radioactivity decay (FIRD) steels for fusion power plant applications are being developed at the Oak Ridge National Laboratory (ORNL) [1]. Induced radioactivity in such steels after neutron irradiation in a fusion plant would decay more rapidly to low levels than would the radioactivity in a similarly irradiated conventional alloy. A reduced-activation alloy cannot contain niobium or molybdenum [2], important constituents in the conventional Cr–Mo steels (e.g., $2\frac{1}{4}$Cr–1Mo, 9Cr–1MoVNb, and 12Cr–1MoVW) that were of interest in the US Fusion program prior to the development of reduced-activation steels.

In the development of FIRD steels at ORNL, eight experimental steels have been studied [3–5]. The compositions of these steels were based on conventional Cr–Mo steels with molybdenum replaced by tungsten and niobium replaced by tantalum [3]. The steels are basically Fe–XCr–2W–0.25V–0.1C (compositions in wt%) with 2.25% Cr (designated $2\frac{1}{4}$Cr–2WV), 5% Cr (5Cr–2WV), 9% Cr (9Cr–2WV), and 12% Cr (12Cr–2WV). Also, compositions with 2.25% Cr and 0% W ($2\frac{1}{4}$CrV), 1% W ($2\frac{1}{4}$Cr–1WV), and 0% V ($2\frac{1}{4}$Cr–2W) were studied along with the 9Cr–2WV steel to which 0.07% Ta was added (9Cr–2WVTa). Nominal compositions are given in Table 1.

Information on microstructure [3], tempering behavior and tensile properties [4], and Charpy impact properties [5] of the eight FIRD steels in the normalized-and-tempered condition has been reported. Results were also published on the tensile properties after irradiation at 365°C to 6–8 and 25–29 dpa and on the Charpy impact properties after irradiation at 365°C to 6–8, 15–17, 23–24, and 26–29 dpa in the Fast Flux Test Facility (FFTF) [6]. The results showed that the two 9Cr steels,

* Corresponding author. Tel.: +1-423 574 5111; fax: +1-423 574 0641; e-mail: ku2@ornl.gov.

[1] Research sponsored by the Office of Fusion Energy Sciences, US Department of Energy, under contract DE-AC05-960R22464 with Lockheed Martin Energy Research Corporation.

0022-3115/99/$ – see front matter
PII: S0022-3115(98)00750-8

Table 1
Nominal compositions for reduced-activation steels

Alloy	Nominal chemical composition [a] (wt %)				
	Cr	W	V	Ta	C
2.25CrV	2.25		0.25		0.1
2.25Cr–1WV	2.25	1.0	0.25		0.1
2.25Cr–2W	2.25	2.0			0.1
2.25Cr–2WV	2.25	2.0	0.25		0.1
5Cr–2WV	5.0	2.0	0.25		0.1
9Cr–2WV	9.0	2.0	0.25		0.1
9Cr–2WVTa	9.0	2.0	0.25	0.12	0.1
12Cr–2WV	12.0	2.0	0.25		0.1

[a] Balance iron.

especially the 9Cr–2WVTa, had superior tensile and Charpy impact properties in both the unirradiated and irradiated conditions, as compared to the other steels. The $2\frac{1}{4}$Cr–2WV steel was the strongest of the eight steels [4], but it had relatively poor impact properties, as was true for the impact properties of all of the low-chromium ($2\frac{1}{4}$Cr) steels [5].

For ferritic steels, the heat treatment determines the microstructure, and the heat treatment designation includes the cooling rate, which is determined by the cooling medium (air, water, oil, etc.) and section size. This paper reports on the effect of irradiation on the Charpy impact properties of the eight ORNL steels after two different heat treatments: one treatment was the same as that used for previous irradiations [6]; in the second heat treatment, the steels were cooled more rapidly during normalization to produce 100% bainite in the $2\frac{1}{4}$Cr steels. Observations on Charpy impact properties after irradiation are useful because neutron irradiation causes an increase in the ductile–brittle transition temperature (DBTT) and a decrease in upper-shelf energy (USE). Such changes generally reflect a degradation in fracture toughness. Developing steels with minimal changes in DBTT and USE is crucial if ferritic steels are to be useful structural materials for fusion.

2. Experimental procedure

Eight electroslag-remelted heats of FIRD steel with the nominal compositions and alloy designations of Table 1 were prepared by Combustion Engineering, Inc, Chattanooga, TN. In addition to nominal compositions of Cr, W, V, C, and Ta (Table 1), elements normally found in such steels (e.g., Mn, Si, etc.,) were adjusted to levels typical of commercial practice. These steels were used in previous studies, and melt compositions have been published [3].

The steels were normalized and tempered prior to irradiation. The $2\frac{1}{4}$Cr–2W steel without vanadium was austenitized at 900°C. The other seven heats contained vanadium and were austenitized at 1050°C; the higher normalizing temperature assured that any vanadium carbide dissolved during austenitization. To determine heat treatment (microstructural) effects, two different geometries were normalized. First, 15.9-mm-thick plates were austenitized 1 h and then air cooled. This is the same heat treatment (termed HT1) used in previous studies [3–6]. In the second heat treatment (HT2), 3.3-mm-square bars (the miniature Charpy specimens) were austenitized 0.5 h in a tube furnace in a helium atmosphere and then pulled into the cold zone of the furnace and cooled in flowing helium. For both HT1 and HT2, the $2\frac{1}{4}$CrV, $2\frac{1}{4}$Cr–1WV, and $2\frac{1}{4}$Cr–2W steel specimens were tempered 1 h at 700°C and the other five heats 1 h at 750°C.

One-third-size Charpy specimens measuring $3.3 \times 3.3 \times 25.4$ mm with a 0.51-mm-deep 30°V-notch and a 0.05- to 0.08-mm-root radius were machined from normalized-and-tempered 15.9-mm plates. Specimens were machined with the longitudinal axis along the rolling direction and the notch transverse to the rolling direction (L-T orientation). The absorbed energy vs. temperature values were fit with a hyperbolic tangent function to permit the USE and DBTT to be consistently evaluated. The DBTT was determined at an energy level midway between the upper- and lower-shelf energies. Details on the test procedure for the subsize Charpy specimens have been published [8].

Six Charpy specimens of each heat and each heat-treated condition were irradiated in the Materials Open Test Assembly of FFTF at ≈393°C. Fluence was determined from flux monitors in the irradiation canisters; there was some variation for different specimens, depending on their position in the canister. Specimens were irradiated to $\approx 2.3 \times 10^{26}$ n/m^2 ($E > 0.1$ MeV), which produced ≈14 dpa. Helium concentrations were calculated to be less than 1 appm.

3. Results

3.1. Microstructures

Microstructures of the normalized-and-tempered 15.9-mm plates (HT1) were examined. Of the low-chromium steels, all but the $2\frac{1}{4}$Cr–2W contained a duplex structure of tempered bainite and polygonal ferrite: $2\frac{1}{4}$CrV (Fig. 1(a)) contained ≈30% tempered bainite, 70% ferrite; $2\frac{1}{4}$Cr–1WV (Fig. 1(b)) contained ≈55% tempered bainite, 45% ferrite; and $2\frac{1}{4}$Cr–2WV (Fig. 1(d)) was ≈80% tempered bainite, 20% ferrite. The $2\frac{1}{4}$Cr–2W steel (Fig. 1(c)) was 100% tempered bainite. When the 3.3-mm bars were heat treated (HT2), the microstructures for all four $2\frac{1}{4}$Cr steels were 100% bainite.

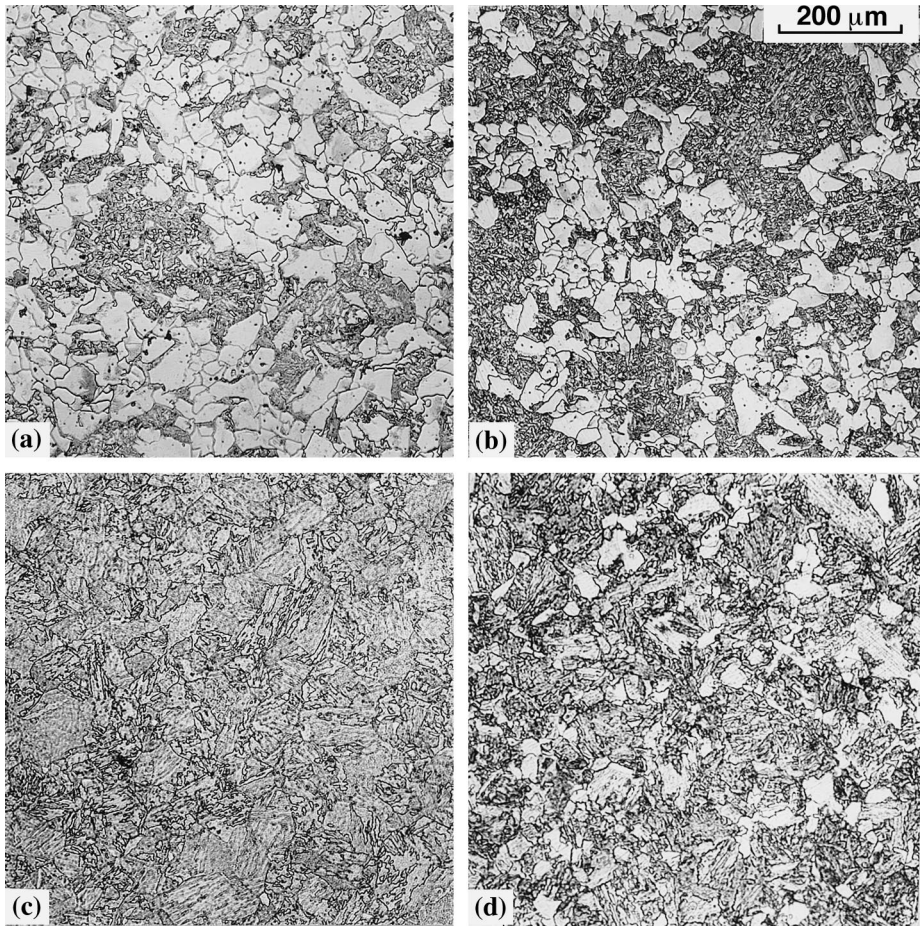

Fig. 1. Microstructures of normalized-and-tempered 15.9-mm-thick plates (HT1) of (a) $2\frac{1}{4}$CrV, (b) $2\frac{1}{4}$Cr–1WV, (c) $2\frac{1}{4}$Cr–2W, and (d) $2\frac{1}{4}$Cr–2WV steels.

Microstructures were the same for the high-chromium steels when heat treated in either geometry: the 5Cr–2WV (Fig. 2(a)), 9Cr–2WV (Fig. 2(b)), and 9Cr–2WVTa (Fig. 2(c)) steels were 100% tempered martensite, and the 12Cr–2WV (Fig. 2(d)) steel was tempered martensite with ≈25% δ-ferrite [3].

3.2. Charpy impact properties

Heat treatment to produce a 100% bainite microstructure (HT2) improved the DBTT of the $2\frac{1}{4}$Cr steels over those with the duplex structure (HT1) (Table 2 and Fig. 3). However, after irradiation, there was little difference in the DBTT of specimens given the HT1 and HT2 heat treatments and, in some cases, the shift in DBTT (ΔDBTT) was higher after HT2 – especially for the $2\frac{1}{4}$Cr–2WV steel (Table 2). Likewise, there was no large difference in the USE after irradiation of $2\frac{1}{4}$Cr steels with HT2 than for those with HT1.

Results for the high-chromium (5–12% Cr) steels were somewhat more varied (Table 2 and Fig. 4). For the 5Cr–2WV steel, HT2 caused a significant improvement in the DBTT over that for HT1 (from −70°C to −112°C), which translated into an improved ΔDBTT for the steel given HT2. Heat treatment had relatively little effect on the DBTT of the two 9Cr steels, either before or after irradiation. The DBTT of the 12Cr–2WV steel specimens given HT1 and HT2 heat treatments were quite similar before irradiation and had similar ΔDBTTs after irradiation. Heat treatment also had little effect on the USE of the high-chromium martensitic steels.

4. Discussion

This irradiation experiment had two objectives: (1) determine whether the microstructure of the $2\frac{1}{4}$Cr steels could be changed by heat treatment to favorably affect

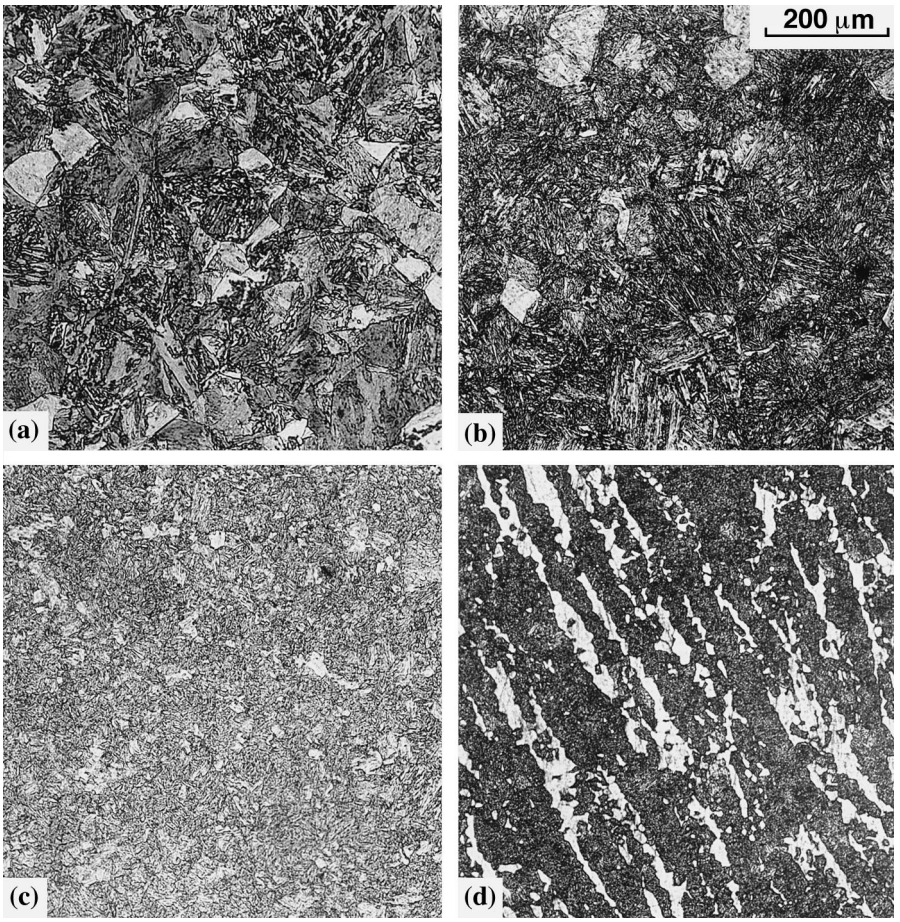

Fig. 2. Normalized-and-tempered microstructures of 15.9-mm-thick plates (HT1) of (a) 5Cr–2WV, (b) 9Cr–2WV, (c) 9Cr–2WVTa, and (d) 12Cr–2WV steels.

the Charpy impact properties after irradiation and (2) irradiate these steels in FFTF at a temperature other than 365°C, the temperature of previous irradiations [6]. The different heat treatments were not expected to cause significant changes in the microstructures of the 5–12% Cr steels, since the high hardenability of these steels would be expected to give them the same martensitic microstructure for both heat treatments. Specimens irradiated at 393°C in this experiment were expected to have a smaller ΔDBTT than those irradiated at 365°C [6], since the shift is due to irradiation hardening and irradiation hardening decreases with increasing irradiation temperature.

The relatively high DBTT values for the $2\frac{1}{4}$CrV, $2\frac{1}{4}$Cr–1WV, and $2\frac{1}{4}$Cr–2WV steels from the 15.9-mm plate (HT1) before irradiation were tentatively attributed to the ferrite in the mixed ferrite-bainite structures [5]. Only the $2\frac{1}{4}$Cr–2W steel had a low DBTT, and it was 100% tempered bainite [5]. Subsequent work [7] indicated that heat treatment affected the unirradiated properties of three of the $2\frac{1}{4}$Cr steels, as it did in the present work (see Table 2) [7]. The DBTT of the 3.3-mm bar of $2\frac{1}{4}$Cr–2W steel, which had the same bainitic microstructure for each heat treatment, was relatively unchanged: −48°C when heat treated as 15.9-mm plate (HT1) and −56°C when heat treated as 3.3-mm bar (HT2). For the other three $2\frac{1}{4}$Cr steels, the specimens given HT2 had considerably lower DBTT values than those given HT1 (Fig. 3(a)). Thus, the previous conclusion that high DBTT values were caused by the ferrite in the mixed ferrite–bainite microstructure of the unirradiated steels appears to be correct [7].

The previous results for the normalized-and-tempered $2\frac{1}{4}$Cr steels suggested that if it were possible to either use thinner sections, quench instead of normalizing, or improve the hardenability of the steels, it might be possible to lower the DBTT to make these steels attractive for fusion reactor applications [7]. The results of the present experiment indicate that it is somewhat more complicated than that when the steels are irradiated.

Table 2
Charpy impact properties of reduced-activation steels irradiated at 393°C

Steel	Heat treatment [a]	DBTT (°C)	ΔDBTT (°C)	USE (J)	ΔUSE (%)
$2\frac{1}{4}$CrV	HT1	36		9.4	
	HT1 – Irrd	287	251	1.4	−85
	HT2	−24		10.9	
	HT2 – Irrd	261	285	2.4	−78
$2\frac{1}{4}$Cr–1WV	HT1	−5		9.7	
	HT1 – Irrd	216	221	2.4	−75
	HT2	−32		9.0	
	HT2 – Irrd	228	260	3.2	−64
$2\frac{1}{4}$Cr–2W	HT1	−48		9.6	
	HT1 – Irrd	176	224	5.0	−48
	HT2	−56		11.5	
	HT2 – Irrd	155	211	8.8	−23
$2\frac{1}{4}$Cr–2WV	HT1	0		9.7	
	HT1 – Irrd	138	138	8.0	−18
	HT2	−52		11.0	
	HT2 – Irrd	152	204	4.8	−56
5Cr–2WV	HT1	−80		10.0	
	HT1 – Irrd	111	191	8.0	−20
	HT2	−112		11.7	
	HT2 – Irrd	21	133	8.0	−32
9Cr–2WV	HT1	−60		9.4	
	HT1 – Irrd	−28	43	8.0	−15
	HT2	−63		9.5	
	HT2 – Irrd	−14	49	8.1	−15
9Cr–2WVTa	HT1	−88		9.7	
	HT1 – Irrd	−45	43	8.9	−8
	HT2	−80		10.1	
	HT2 – Irrd	−53	27	8.4	−17
12Cr–2WV	HT1	−50		9.0	
	HT1 – Irrd	83	133	6.0	−33
	HT2	−59		9.9	
	HT2 – Irrd	77	136	5.7	−42

[a] HT1: normalized and tempered as 15.9-mm plate; HT2: normalized and tempered as 3-mm bar; Irrd: irradiated to ≈14 dpa.

Despite the decrease in DBTT caused by HT2 compared with that for HT1, there was no advantage for HT2 after irradiation.

It was previously shown that the bainite that forms in the $2\frac{1}{4}$Cr steels is not the same in all four steels [7]. Bainite, which is generally defined as a ferrite matrix containing carbides that forms in the temperature range 250–550°C, was originally thought to have only two morphological variations – upper and lower bainite [9]. Classical upper and lower bainite can be differentiated by the appearance of the carbide particles relative to the axis of the bainitic ferrite plate or needle. Upper bainite forms as a collection of ferrite plates or laths with carbides forming on the boundaries between the plates or laths. Lower bainite consists of ferrite plates or needles with carbides forming within the ferrite plates or needles at about a 60° angle to the axis of the plate or needle [9].

There are important variations on the classical bainites, as first shown by Habraken [10]. He found morphological variants in the bainite transformation products that differed from upper and lower bainite, although these products formed in the bainite transformation temperature regime. These 'non-classical' bainites formed more easily during a continuous cool than during isothermal transformation [10,11], where classical bainites are generally formed.

Habraken and Economopoulos contrasted the morphology of the nonclassical structures formed during continuous cooling with classical bainites obtained during isothermal transformation [11]. Classical upper and lower bainites form when the steel is transformed in different temperature regimes of the bainite transformation temperature region, as defined on an isothermal-transformation (IT) diagram [11]. This means that the bainite transformation region of an IT diagram can be divided into two temperature regimes by a horizontal line, above which upper bainite forms and below which lower bainite forms. For the nonclassical bainites, Habraken and Economopoulos [11] showed that a continuous cooling transformation (CCT) diagram could be divided into three vertical regions. Three different nonclassical bainite microstructures form when cooling rates

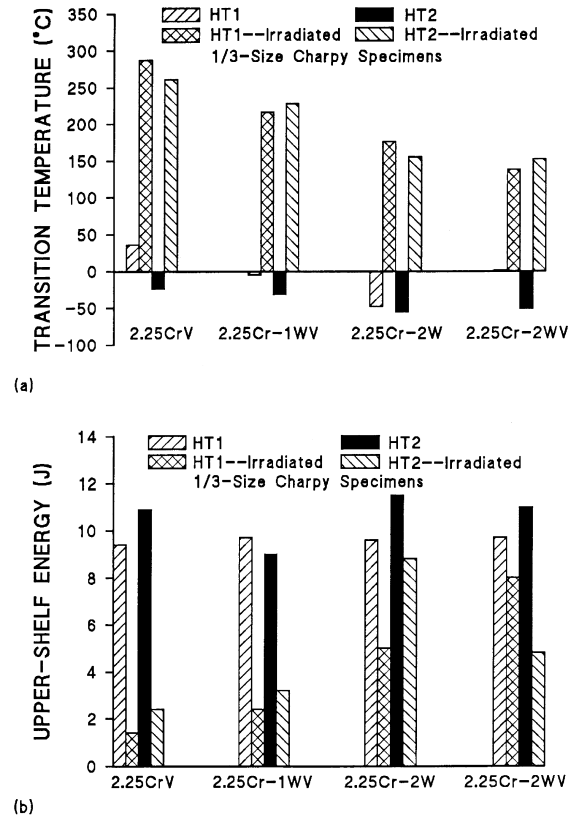

Fig. 3. The (a) transition temperature and (b) upper-shelf energy for the low-chromium (2.25% Cr) steels given two different normalizing and tempering treatments (HT1 and HT2) and after these two heat treated conditions were irradiated to ≈14 dpa at 393°C.

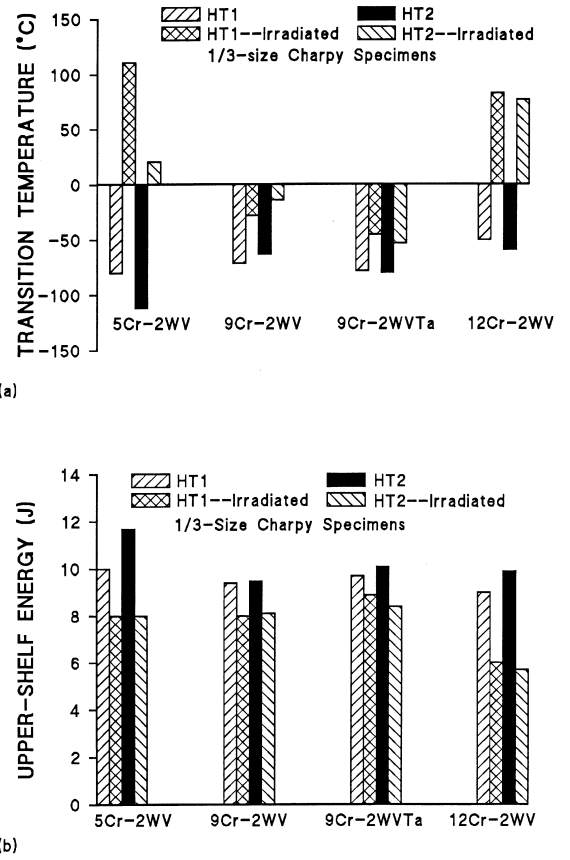

Fig. 4. The (a) transition temperature and (b) upper-shelf energy for the high-chromium (5–12% Cr) steels given two different normalizing and tempering treatments (HT1 and HT2) and after these two heat treated conditions were irradiated to ≈14 dpa at 393°C.

are such as to pass through these different zones. Two of those microstructures are of interest here.

A steel cooled rapidly enough to pass through the first zone produces a 'carbide-free acicular' structure, which consists of side-by-side plates or laths [11]. When cooled somewhat more slowly through the second zone, a carbide-free 'massive or granular' structure results, generally referred to as granular bainite [11]. Granular bainite consists of a ferrite matrix with a high dislocation density that contains martensite–austenite (M–A) 'islands' [11].

Microstructures in the 15.9-mm plates of the $2\frac{1}{4}$Cr–2W and $2\frac{1}{4}$Cr–2WV consisted of carbide-free acicular bainite and granular bainite, respectively [7]. During tempering, large globular carbides form in the M–A islands of the granular bainite, whereas elongated carbides form on lath boundaries of acicular bainite [7]. When the 3-mm bars were normalized, carbide-free acicular bainite also formed in the $2\frac{1}{4}$Cr–2WV steel [7]. Although no TEM was performed on the $2\frac{1}{4}$CrV and $2\frac{1}{4}$Cr–1WV, a similar microstructure is expected for these steels.

The results for the $2\frac{1}{4}$Cr steels in the present experiment indicate that neither the carbide-free acicular structure obtained by heat treating the 3-mm bars nor the granular bainite previously irradiated provides a microstructure that has good resistance to irradiation-induced embrittlement. The large globular carbides that form in granular bainite may provide crack initiation sites in the normalized-and-tempered condition. Carbides in ferritic steels can grow during irradiation [12], which may lead to the lack of resistance to irradiation-induced embrittlement observed in these steels. Likewise, the interlath carbides developed in the acicular bainite during tempering can be quite large and may provide crack initiation sites.

Because the $2\frac{1}{4}$Cr–2WV steel was the strongest of the eight steels in the unirradiated condition and because it is possible to produce a high density of small precipitates

in a low-chromium steel that cannot be produced in a high-chromium steel (considering concentrations similar to those in Table 1), it has been suggested that the low-chromium steels may offer some advantages for fusion [3,7]. Results from the present experiment appear to contradict that suggestion – certainly for the compositions and heat treatments used here.

The acicular structures of the 2.25% Cr steels irradiated in the present work contained fairly large intra- and inter-lath M_3C and M_7C_3 carbides that formed during tempering [3,7]. These carbides may provide crack initiation sites for fracture. If this is the case, a more irradiation-resistant microstructure might be achieved by cooling still more rapidly to minimize carbon segregation during cooling and thus prevent the formation of large carbides during tempering. An alternative to rapid cooling is to increase the hardenability. This can be done by changing the chemical composition, and a 3Cr–3WV steel has been developed that shows a significant improvement in the Charpy impact properties in the unirradiated condition [13]. This superiority was present even when tempered at 700°C or in the untempered condition. However, the irradiation resistance of this steel still needs to be determined.

Because of the high hardenability of the high-chromium (5–9% Cr) martensitic steels, no effect of cooling rate on Charpy properties was expected, and none was observed for the 9Cr–2WV, 9Cr–2WVTa, and 12Cr–2WV steels (Table 2 and Fig. 4). Microstructures were unchanged from 100% martensite for the 9Cr steels and 20–25% δ-ferrite with the balance martensite for the 12Cr steel, regardless of the size of specimen heat treated.

Although the microstructure of the 5Cr–2WV steel was 100% martensite and the DBTT of this steel was not expected to change, an effect was seen (a DBTT of −80°C for HT1 and −112°C for HT2). No major difference in the optical microstructures of the unirradiated plate and bar for the high-chromium steels were observed. The prior-austenite grain sizes were similar, although the plate was austenitized 1 h at 1050°C, while the smaller bar was austenitized 0.5 h at 1050°C.

The major difference in the microstructure in the unirradiated condition of the 9Cr and 12Cr steels compared to that of the 5Cr steel is the precipitates. The primary precipitate in the 9Cr and 12Cr steels is $M_{23}C_6$; in the 5Cr steel, it is M_7C_3 [3]. Both steels contain vanadium-rich MC, and the 5Cr steel contains a small amount of $M_{23}C_6$. Some M_7C_3 might precipitate in the 5Cr–2WV steel during the slow cool (in the 15.9-mm plate), and these precipitates could grow to larger sizes during tempering than would be the case if precipitates did not form during normalization. This is strictly speculation, since no transmission electron microscopy (TEM) has been performed on the steels heat treated as 3.3-mm bar in the normalized-and-tempered condition, and there has been no TEM on the 5Cr–2WV after irradiation. The only apparent change observed for the 9Cr steels after irradiation to 36 dpa at 420°C was the formation of dislocation loops estimated to be 40–100 nm in diameter at a number density of $3 \times 10^{15}/cm^3$ [12].

When the DBTT values obtained previously after irradiation to ≈16 dpa at 365°C [6] were compared to those observed after ≈14 dpa at 393°C in the present experiment, the DBTT values of the $2\frac{1}{4}$Cr steels (Fig. 5) and the 12Cr–2WV steel (Fig. 6) were higher (larger ΔDBTT) after irradiation at 365°C than after the irradiation at 393°C. This is expected, since the shift in DBTT is directly related to irradiation hardening, and irradiation hardening decreases with increasing irradiation temperature. Just the opposite occurred for the 5Cr–2WV and the 9Cr–2WVTa steels (Fig. 6). For 5Cr–2WV, the DBTT values were 45°C (16.7 dpa) and 111°C (14 dpa) at 365°C and 393°C, respectively, and for the 9Cr–2WVTa steel, the values were −74°C (15.4 dpa) and

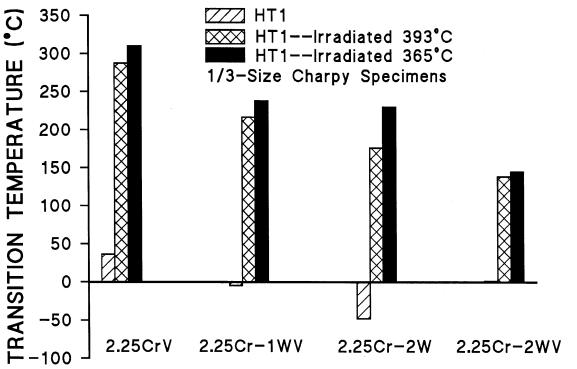

Fig. 5. The transition temperature of the low-chromium (2.25% Cr) steels in HT1 and after irradiation to ≈15 dpa at 365°C and ≈14 dpa at 393°C.

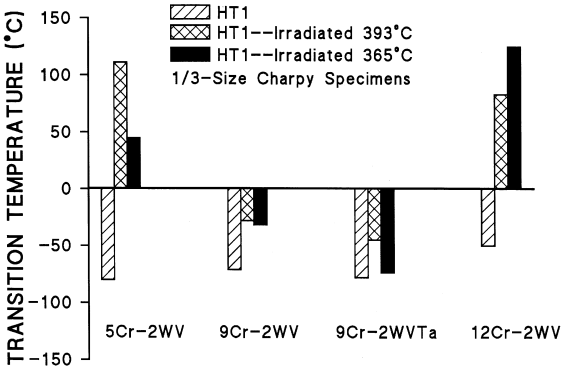

Fig. 6. The transition temperature of the high-chromium (5–12% Cr) steels in HT1 and after irradiation to ≈15 dpa at 365°C and ≈14 dpa at 393°C.

−45°C (14 dpa) at 365°C and 393°C, respectively. There was essentially no difference in the DBTT values of the 9Cr–2WV steel after irradiation at 365°C (16.7 dpa) or at 393°C (14 dpa) (−32°C and −28°C, respectively) (Fig. 6). However, after irradiation at 365°C to 7.7, 23.9, and 27.6 dpa, this steel had DBTT values of 8°C, −8°C, and 1°C, respectively. While it is difficult to reach a firm conclusion with the limited data available and the scatter inherent in impact testing, the saturation value for the DBTT is probably about 0°C, despite the lower value observed for irradiation to 16.7 dpa. Taken together, the available data suggest that the DBTT for 9Cr–2WV steel is somewhat higher after irradiation at 365°C (≈0°C) than for irradiation at 393°C (−28°C). Thus, it is concluded that all but the 5Cr–2WV and 9Cr–2WVTa steels showed the expected decrease in DBTT with increasing irradiation temperature.

To try to understand the inverse temperature effect (a larger ΔDBTT at 393°C than 365°C) for the 5Cr–2WV, it is useful to compare the behavior of the 5Cr–2WV and 9Cr–2WV steels, which differ only in chromium concentration. The major difference in the microstructures of the two steels is the primary precipitates – M_7C_3 in the 5Cr–2WV and $M_{23}C_6$ in the 9Cr–2WV. Carbide particles can act as initiation sites for the brittle cracks that cause the fracture [14,15]. As the size of a brittle precipitate particle increases, so too the size of the initial crack at fracture initiation increases. Thus, a possible reason why the 5Cr steel had a higher DBTT after irradiation at 393°C than at 365°C is that M_7C_3 precipitates can grow to a larger size by irradiation-enhanced diffusion at the higher irradiation temperature. It is the larger precipitates that then cause the inverse temperature effect for this steel. A possible effect of precipitates was also used above to explain the difference in properties for HT1 and HT2 for 5Cr–2WV. TEM is required to verify both suggestions.

If the results for the 5Cr–2WV steel on the effect of heat treatment and irradiation temperature are due to changes in carbide size, this suggests that the DBTT after irradiation can be improved by decreasing the size of these carbide precipitates. Their size would be decreased by lowering the tempering temperature, and previous work has shown that the 5Cr–2WV steel has excellent Charpy properties even after tempering 1 h at 700°C, as opposed to the 750°C used in the present experiment [5]. TEM would again be required to confirm this suggested role of carbide particles.

The 9Cr–2WVTa steel had the best Charpy properties after irradiation of any of the steels tested here, and in other irradiation experiments it was shown to have the lowest radiation sensitivity for this type of steel ever observed [6,16,17]. Again, while it is difficult to reach firm conclusions on the basis of the limited available data, this steel also seems to show an inverse temperature effect. After 15 dpa at 365°C, the ΔDBTT for HT1 was only 14°C compared to 27°C after 14 dpa at 393°C (Table 2).

An inverse temperature effect was also observed previously when the steel was irradiated to 0.8 dpa at 250–450°C in the High Flux Reactor (HFR) in Petten, the Netherlands [16]. Fig. 7 shows the DBTT of the 9Cr–2WVTa steel (labeled ORNL) irradiated in HFR along with several other reduced-activation steels, OPTIFER-Ia (nominally 9.3Cr–1W–0.25V–0.07Ta–0.1C), OPTIFER-II (9.4Cr–1.1Ge–0.3V–0.13C), and F82H (8Cr–2W–0.2V–0.02Ta–0.1C), and two conventional Cr–Mo steels, MANET-I (11Cr–0.8Mo–0.2V–0.9Ni–0.16Nb–0.06Zr–0.14C) and MANET-II (10Cr–0.6Mo–0.2V–0.7Ni–0.14Nb–0.4Zr–0.1C). The ORNL 9Cr–2WVTa steel had the lowest DBTT below ≈375°C [16]. This superior behavior has now been verified for irradiation to 2.5 dpa in HFR [17]. The inverse temperature effect was displayed by the 9Cr–2WVTa steel in that the DBTT increased above 400°C (Fig. 7). This is the temperature regime where hardening is expected to decrease to low values, which should translate to low values of DBTT. Indeed, no such increase was observed for the other steels.

The origin of the superior behavior for the 9Cr–2WVTa has been sought by comparing the behavior of this steel to that of the 9Cr–2WV steel, which is the same as the 9Cr–2WVTa but without tantalum [6]. The 9Cr–2WV and 9Cr–2WVTa steels were irradiated at 365°C in FFTF, with the 9Cr–2WVTa showing exceptionally small ΔDBTTs: 4°C, 14°C, 21°C, and 32°C (DBTTs of −84°C, −74°C, −67°C, and −56°C) after 6.4, 15.4, 22.5, and 27.6 dpa, respectively (the value after 15.4 dpa is plotted in Fig. 6) [6]. The ΔDBTT and DBTT for the 9Cr–2WV saturated at ≈60 and 0°C, respectively, which was reached by ≈8 dpa (the lowest irradiation fluence) [6]. These differences for the HT1 heat treatment

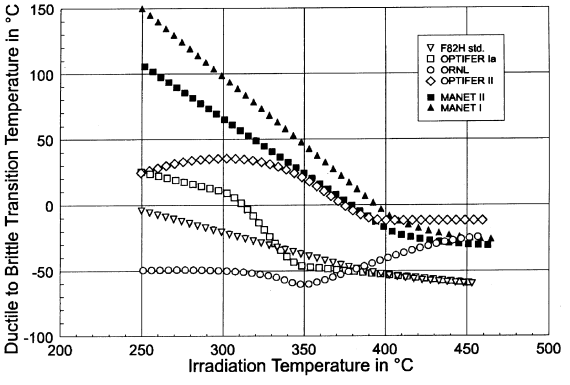

Fig. 7. Trends in the transition temperature as a function of irradiation temperature for miniature Charpy specimens of four reduced-activation and two conventional martensitic steels irradiated at 250°C, 300°C, 350°C, 400°C, and 450°C to 0.8 dpa in the HFR. Taken from Rieth et al. [16].

occurred despite there being little difference in the strength of the two steels before and after irradiation [6].

TEM examination of the normalized-and-tempered 9Cr–2WV and 9Cr–2WVTa revealed only minor differences prior to irradiation [3,12]. The 9Cr–2WVTa did have a smaller prior-austenite grain size (22 μm vs. 32 μm), but both contained similar precipitates and precipitate distribution. Likewise, no marked difference in microstructure was observed after irradiation; similar numbers of dislocation loops formed in both steels [12]. Thus, the similarity in strength of these two steels before and after irradiation is not unexpected. However, without any gross differences in the microstructure of the two steels, the only other major difference to account for the difference in Charpy properties is the tantalum in solid solution. Based on the amount of tantalum that appeared to be present in the MC carbides of the 9Cr–2WVTa steel, it was estimated that most of the tantalum remained in solid solution [12]. A subsequent atom probe analysis of the unirradiated 9Cr–2WVTa steel indicated that >90% of the tantalum was in solution in the normalized-and-tempered condition [18].

Tantalum can probably account for the smaller prior-austenite grain size in the 9Cr–2WVTa than in the 9Cr–2WV. A smaller lath (subgrain) size might also be expected but was not observed in two studies [3,12], although a smaller lath size was observed in a third examination [18]. The smaller prior-austenite grain size was originally used to explain the difference between the 9Cr–2WV and 9Cr–2WVTa steels [19], since a smaller grain size should lead to a lower DBTT in the normalized-and-tempered condition. However, prior-austenite grain size as the sole explanation was subsequently questioned, because in the normalized-and-tempered condition, the two steels had similar yield stresses, and they also had a yield stress similar to that of the conventional 9Cr–1MoVNb (modified 9Cr–1Mo) steel, which had the smallest grain size of the three steels [6]. After similar irradiation of the three steels, the ΔDBTT of the 9Cr–2WV and 9Cr–1MoVNb were similar, but greater than the value for the 9Cr–2WVTa [6]. There were minor differences in the irradiated microstructures of the 9Cr–1MoVNb steel and the other two steels, but there was essentially no difference in the microstructural changes that occurred in the 9Cr–2WV and 9Cr–2WVTa steels [12].

These observations led to the suggestion that microstructure (grain size, precipitate type, etc.) could not provide the sole explanation for the observations on mechanical property changes. It was proposed [19] that tantalum in solution could cause a higher fracture stress for 9Cr–2WVTa than for 9Cr–2WV, and the combination of tungsten and tantalum in the 9Cr–2WVTa could lead to a higher fracture stress than produced by the combination of molybdenum and niobium in 9Cr–1MoVNb steel [6].

In his analysis of brittle fracture, Griffith [20,21] considered the balance between the energy released by elastic relaxation and that required for the creation of new surface area during the growth of a crack in a brittle material; for a through crack, he found that

$$\sigma_f = \left(\frac{2E\gamma_s}{\pi a(1-\nu^2)}\right)^{1/2}, \tag{1}$$

where σ_f is the stress at fracture, E is Young's modulus, γ_s is the true surface energy, ν is Poisson's ratio, and a is the crack half-length. Orowan [22] and Irwin [23] suggested that the true surface energy should be replaced by an effective surface energy, γ_e, which would include the plastic work done during fracture. For an embedded penny-shaped crack, as would result from initiation at a carbide particle or at an inclusion, or from a crack forming within an entire grain or other microstructural unit, this equation becomes [24]

$$\sigma_f = \left(\frac{4E\gamma_e}{D(1-\nu^2)}\right)^{1/2}, \tag{2}$$

where D is the crack diameter. An additional factor can be included to account for elliptically shaped particles [25].

For a ferritic steel with spherical carbide particles, the diameter of the fracture-initiating carbide particle would be used for the crack diameter, D. However, this cannot explain the different responses of 9Cr–2WVTa and 9Cr–2WV steels during irradiation, since there appears to be no significant difference in the amount or morphology of the precipitates in these two steels before or after irradiation [3,12].

The packet or lath size of a bainitic or martensitic steel could be used as the initiating crack size. Although one TEM study found a difference in the lath size of the normalized-and-tempered 9Cr–2WV and 9Cr–2WVTa steels (the 9Cr–2WVTa had a smaller lath size) [18], two other studies found no difference [3,12], possibly indicating a non-uniform microstructure, as is often the case for these steels. There was no apparent difference in lath size of the two steels after irradiation to 36 dpa at 420°C in FFTF [12]. That is, the lath size for both steels showed a similar increase – if they had similar lath sizes before and after irradiation – or the 9Cr–2WVTa steel showed a larger increase in lath size – if it had a smaller lath size prior to irradiation. Therefore, lath size does not offer an explanation (the two steels would show a similar ΔDBTT for a similar increase in lath size, or the 9Cr–2WVTa would show a larger ΔDBTT for a larger change if the lath size of this steel was smaller prior to irradiation).

Prior-austenite grain size could also be considered as the crack size, but this does not explain the change in DBTT because prior austenite grain size does not change during irradiation.

After eliminating carbides, lath size, and prior austenite grain size as explanations for the observations on 9Cr–2WVTa, Eq. (2) indicates that the explanation must involve Young's modulus or the effective surface energy. The small amount of tantalum added should have no appreciable effect on the elastic modulus. Gerberich et al. found effects of nickel and silicon on the effective surface energy for binary iron-based alloys [26]. They concluded that a change in the fracture stress could explain why nickel caused a decrease and silicon caused an increase in the transition temperature of binary Fe–Ni and Fe–Si alloys. Since microstructural changes (grain size, precipitate type, etc.) cannot provide the sole explanation for the observations on mechanical property changes for the 9Cr–2WVTa, it appears one possible explanation is that tantalum in solution may change the effective surface energy, which causes a higher fracture stress for the 9Cr–2WVTa than the 9Cr–2WV, and the combination of tungsten and tantalum in the 9Cr–2WVTa steel leads to a higher fracture stress than produced by molybdenum and niobium in 9Cr–1MoVNb steel [6].

The transition temperature also depends on flow stress. It is the increase in flow stress during irradiation that causes the increase in transition temperature. The DBTT depends on the intercept of the flow stress–temperature curve with the fracture stress–temperature curve [27]. Fracture becomes brittle when the cleavage fracture stress becomes less than the yield stress. Therefore, as an alternative to tantalum causing an increase in fracture stress, the observed effect of tantalum could be due to its effect on the flow stress–temperature or flow stress–strain rate relationships, which could affect the DBTT and ΔDBTT. Previously, it was assumed that because the 9Cr–2WV and 9Cr–2WVTa had similar yield stresses between room temperature and 600°C, there was no effect of tantalum on the flow stress–temperature relationship [19]. This ignores the possibility that there could be a tantalum effect at low temperatures or high strain rates. In the future, this possibility will be investigated, since this effect is easier to investigate than the fracture stress.

The effects of microstructural parameters on the transition temperature are complex, as Gerberich et al. [26] have noted; the ductile–brittle transition model for iron and iron-binary alloys that they derived involved 19 flow and fracture parameters.

If it is assumed that tantalum in solution changes the fracture stress or flow stress, then the anomalous behavior of the 9Cr–2WVTa steel can be explained. The observation that the ΔDBTT of the 9Cr–2WVTa appeared to increase continuously with fluence instead of saturating when irradiated at 365°C [6] would follow if tantalum is being removed from solution during irradiation and being incorporated in the existing or new precipitates. Precipitation can also explain the increase in DBTT for the 9Cr–2WVTa irradiated above about 400°C in HFR (Fig. 7). The increase occurs at $\gtrsim$400°C where irradiation-enhanced diffusion, even after only 0.8 dpa, may accelerate the reduction of tantalum in solution. The same reason explains the better properties observed after irradiation to 15 dpa at 365°C than after 14 dpa at 393°C in the present experiment (Fig. 6). That is, more tantalum is being removed from solution at the higher irradiation temperature. If this is the case, the ΔDBTT of the 9Cr–2WVTa would be expected to increase with fluence as tantalum is removed from solution, just as is observed at 365°C [6]. Eventually, it might be expected to approach the ΔDBTT for the 9Cr–2WV, because as the tantalum is removed from solution, the matrix of the two steels should become similar. That appears to be happening (Table 2). The ΔDBTT for 9Cr–2WV and 9Cr–2WVTa are both 43°C for HT1; for HT2, the ΔDBTT is 49°C for 9Cr–2WV and 27°C for 9Cr–2WVTa. This compares with ΔDBTT values of ≈70°C and ≈30°C for the 9Cr–2WV and 9Cr–2WVTa steels, respectively, after ≈28 dpa at 365°C in FFTF [6]. Even after the ΔDBTTs become the same for the two steels, however, the 9Cr–2WVTa still has the lower DBTT after irradiation because of its lower DBTT before irradiation [6]. This is probably a consequence of the smaller prior-austenite grain size of the 9Cr–2WVTa steel.

5. Summary and conclusion

Charpy impact properties were determined on eight reduced-activation Cr–W ferritic steels irradiated in FFTF to ≈14 dpa at 393°C. To determine the effect of heat treatment (cooling rate), specimens were taken from normalized-and-tempered 15.9-mm plate and 3.3-mm bar. Chromium concentrations in the steels ranged from 2.25 to 12 wt% (all steels contained 0.1%C). The $2\frac{1}{4}$Cr steels contained variations of tungsten and vanadium ($2\frac{1}{4}$CrV, $2\frac{1}{4}$Cr–1WV, $2\frac{1}{4}$Cr–2W) and steels with 2.25%, 5%, 9%, and 12% Cr contained a combination of 2% W and 0.25% V ($2\frac{1}{4}$Cr–2WV, 5Cr–2WV, 9Cr–2WV, and 12Cr–2WV). A 9Cr steel containing 2% W, 0.25% V, and 0.07% Ta (9Cr–2WVTa) was also irradiated. The microstructure of the $2\frac{1}{4}$Cr steels in the 15.9-mm plate were bainite with various amounts of polygonal ferrite, and they were 100% bainite when heat treated as 3.3-mm bar. The 5Cr steel and the two 9Cr steels were 100% martensite and the 12Cr steel was martensite with ≈25% δ-ferrite after heat treatment in either geometry.

The change in microstructure caused by heat treatment of the $2\frac{1}{4}$Cr steels from duplex microstructures of bainite plus ferrite to 100% bainite resulted in improvement in the Charpy impact properties before irradiation. After irradiation, however, there was little difference in the properties for the two different heat treatments. As

expected, cooling rate had little effect on the high-chromium (9% and 12% Cr) steels. The Charpy properties for the 5Cr–2WV steel were improved by the faster cooling rate of the 3.3-mm bar. The reason for this change is unclear, but perhaps it may be due to the different precipitates present in the 5Cr steel as compared to the other martensitic steels (M_7C_3 is present in the 5Cr–2WV steel but not in the other martensitic steels).

Results from the present irradiation experiment were compared with previous experiments for irradiation at a lower temperature (365°C) but similar dpa levels. The DBTT values of all but the 5Cr–2WV and 9Cr–2WVTa steels were lower after irradiation at 393°C than after irradiation at 365°C, which is the expected behavior. The contrary behavior of the 5Cr steel was tentatively attributed to the M_7C_3 carbides that form in this composition that are not present in the 9Cr and 12Cr steels. The inverse temperature effect in the 9Cr–2WVTa steel was suggested to be due to the loss of tantalum from solution during irradiation at the higher temperature. Tantalum in solution may give the 9Cr–2WVTa steel its advantage over the other steels by increasing the cleavage fracture stress or changing the flow stress-temperature relationship, and this advantage is decreased by the precipitation of tantalum from solution during irradiation. However, a thorough analytical TEM examination of these steels is required to confirm the suggested mechanism.

Acknowledgements

We wish to thank E.T. Manneschmidt for conducting the impact tests and R.K. Nanstad and J.P. Robertson for reviewing the manuscript. Also acknowledged is the anonymous reviewer who pointed out that the possibility of a tantalum effect on flow stress should be considered in our explanation of the observations.

References

[1] R.L. Klueh, K. Ehrlich, F. Abe, J. Nucl. Mater. 191–194 (1992) 116.
[2] R.W. Conn et al., Panel Report on Low Activation Materials for Fusion Applications, University of California, Los Angeles, PPG-753, March 1983.
[3] R.L. Klueh, P.J. Maziasz, Metall. Trans. 20A (1989) 373.
[4] R.L. Klueh, Metall. Trans. 20A (1989) 463.
[5] R.L. Klueh, W.R. Corwin, J. Mater. Eng. 11 (1989) 169.
[6] R.L. Klueh, D.J. Alexander, in: R.K. Nanstad, M.L. Hamilton, F.A. Garner, A.S. Kumar (Eds.), Effects of Radiation on Materials: 18th International Symposium, ASTM STP 1325, American Society for Testing and Materials, Philadelphia (to be published).
[7] R.L. Klueh, P.J. Maziasz, D.J. Alexander, J. Nucl. Mater. 179–181 (1991) 679.
[8] D.J. Alexander, R.K. Nanstad, W.R. Corwin, J.T. Hutton, in: A.A. Braun, N.E. Ashbaugh, F.M. Smith (Eds.), Applications of Automation Technology to Fatigue and Fracture Testing, ASTM STP 1092, American Society for Testing and Materials, Philadelphia, 1990, p. 83.
[9] R.W.K. Honeycombe, Steels: Microstructures and Properties, Edward Arnold Ltd, London, 1981, p. 106.
[10] L.J. Habraken, Proc. Fourth Intl. Conf. Electron Microscopy, vol. 1, Springer, Berlin, 1960, p. 621.
[11] L.J. Habraken, M. Economopoulos, Transformation and Hardenability in Steels, Climax-Molybdenum Company, Ann Arbor, MI, 1967, p. 69.
[12] J.J. Kai, R.L. Klueh, J. Nucl. Mater. 230 (1996) 116.
[13] R.L. Klueh, D.J. Alexander, P.J. Maziasz, Metall. Trans. 28A (1997) 335.
[14] R.W. Hertzberg, Deformation and Fracture Mechanics of Engineering Materials, 3rd ed., Wiley, New York, 1989, p. 253.
[15] C.J. McMahon Jr., in: L.J. Bonis, J.J. Duga, J.J. Gilman (Eds.), Fundamental Phenomena in the Materials Sciences, vol. 4, Plenum, New York, 1967, p. 247.
[16] M. Rieth, B. Dafferner, H.D. Röhrig, J. Nucl. Mater. 233–237 (1996) 351.
[17] M. Rieth, B. Dafferner, H.D. Röhrig, J. Nucl. Mater. (to be published).
[18] R. Jayaram, R.L. Klueh, Metall. Mater. Trans. 29A (1998) 1551.
[19] R.L. Klueh, D.J. Alexander, J. Nucl. Mater. 212–215 (1994) 736.
[20] A.A. Griffith, Philos. Trans. R. Soc. London 221A (1920) 163.
[21] A.A. Griffith, Proc. First Int. Cong. Appl. Math., Delft, The Netherlands, 1924, p. 55.
[22] E. Orowan, Rep. Prog. Phys. 12 (1948–1949) 185.
[23] G.R. Irwin, in: Fracture of Metals, American Society for Metals, Cleveland, OH, 1948, p. 147.
[24] R.A. Sack, Proc. Phys. Soc. London 58 (1946) 729.
[25] H.L. Ewalds, R.J.H. Wanhill, Fracture Mechanics, Edward Arnold Ltd, London, 1984, p. 43.
[26] W.W. Gerberich, Y.T. Chen, D.G. Atteridge, T. Johnson, Acta Metall. 29 (1981) 1187.
[27] J.R. Hawthorne, Treatise Mater. Sci. Tech. 25 (1983) 461.